Electronic Supplementary Material (ESI) for Journal of Materials Chemistry A.

SUPPLEMENTARY INFORMATION

Hydroxyapatite-based Catalysts for CO_2 Fixation with Controlled Selectivity Towards C2 Products. Phenomal Support or Active Catalyst?

Marc Arnau,[1,2] Pau Turon,[3] Carlos Alemán[1,2,4*] and Jordi Sans[1,2*]*

[1] *Departament d'Enginyeria Química, EEBE, Universitat Politècnica de Catalunya, C/ Eduard Maristany, 10-14, Ed. I2, 08019, Barcelona, Spain*

[2] *Barcelona Research Center in Multiscale Science and Engineering, Universitat Politècnica de Catalunya, C/ Eduard Maristany, 10-14, 08019, Barcelona, Spain*

[3] *B. Braun Surgical, S.A. Carretera de Terrasa 121, 08191 Rubí (Barcelona), Spain*

[4] *Institute for Bioengineering of Catalonia (IBEC), The Barcelona Institute of Science and Technology, Baldiri Reixac 10-12, 08028 Barcelona Spain*

[*] Correspondence to: pau.turon@upc.edu, carlos.aleman@upc.edu and jordi.sans.mila@upc.edu

METHODS

Materials

Ammonium phosphate dibasic [$(NH_4)_2HPO_4$; purity ≥ 99.0%] and ammonium hydroxide solution 30% (NH_4OH; purity: 28-30%), Calcium nitrate tetrahydrate $CaN_2O_6 \cdot 4H_2O$ (ACS reagent, 99-103%) and Dulbecco's Phosphate Buffered Saline (PBS) were purchased from Sigma-Aldrich. Commercial TiO_2 nanoparticles (P90) were purchased from Degussa. Ethanol CH_3CH_2OH (purity ≥ 99.8%) which was purchased from Honeywell and de-ionized water was provided by MILLI-Q® Water Purification System from MILLIPORE S.A.

Synthesis of hydroxyapatite (HAp)

15 mL of 0.5 M $(NH_4)_2HPO_4$ in de-ionized water were added at a rate of 2 mL/min to 25 mL of a 0.5 M of $Ca(NO_3)_2$ solution in ethanol with pH previously adjusted to 11 using ammonium hydroxide solution. The mixture was left aging for 1 h under gentle agitation (150 rpm) at room temperature. Hydrothermal treatment at 150 ºC was applied using an autoclave Digestec DAB–2 for 24 h. The autoclave was allowed to cool down before opening. The precipitates were separated by centrifugation and washed with water and a 60/40 v/v mixture of ethanol/water (twice) using a Sorvall RC 5B PLUS (modulus SS-34). After lyophilizing it for 3 days (Telstar LyoQuest), a white HAp powder was obtained.

Thermal stimulation polarization (TSP) treatment

HAp discs, which were obtained by pressing 150 mg of s-HAp powder at 620 MPa for 10 min, after TiO_2 NP loading by means of drop casting, were catalytically activated by placing the samples between two stainless steel plates (AISI 304) separated ~4cm and

applying a constant DC voltage of 500 V for 1 h with a GAMMA power supply, while temperature was kept at 1000 ºC. Samples were allowed to cool down maintaining the applied electric potential for 30 minutes, and finally, all the system was powered off and left to cool down overnight.

Characterization

Raman analyses were performed by means of an inVia Qontor confocal Raman microscope (Renishaw) equipped with a Renishaw Centrus 2957T2 detector and a 532 nm laser. In order to obtain representative data, 32 single point spectra were averaged.

Wide angle X-ray diffraction (WAXD) studies were conducted using a Brucker D8 Advance model with Bragg-Brentano 2θ configuration and Cu K_α radiation (λ = 0.1542 nm). Measurements were performed in a 2θ range of 20º–60º in steps of 0.02º and scan speed of 2 s, using a one-dimensional Lynx Eye detector.

Samples were analysed using XPS on a SPECS system. The spectrometer was equipped with a high-intensity twin-anode X-ray source XR50 of Mg/Al (1253 eV/ 1487 eV) operating with the Al anode at 150 W, placed perpendicular to the analyser axis, and using a Phoibos 150 MCD-9 XP detector. The position of the stage was digitally controlled to ensure that the spot was in the same exact place during the whole treatment. The pass energy of the hemispherical analyser was set at 25 eV and the energy step of high resolution spectra was set at 0.1 eV. The pressure in the analysis chamber was always below 10^{-7} Pa, and binding energy (BE) values were referred to the C 1s peak at 284.8 eV.

Dynamic Light Scattering (DLS) measurements were performed on a NanoBrook 90Plus Zeta set to collect and average data every 3 minutes. Samples were suspended (37.1

mg/L) in a PBS (4.8 g/L) aqueous solution and sonicated for 10 min before each measurement. All experiments were performed at room temperature conditions.

Morphological characterization was performed by scanning electron microscopy (SEM) using a Focused Ion Beam Zeiss Neon40 microscope equipped with a SEM GEMINI column with a Shottky field emission. Images were acquired with both backscattered and secondary electrons detectors. Samples were sputter-coated with a thin layer of carbon to prevent sample charging problems.

High-resolution transmission electron experiments were carried out in a JEOL JEM J2100 microscope, equipped with a LaB6 thermionic electron gun and operated at an accelerating voltage of 200 keV. Images were recorded using a Gatan Orius CCD camera.

Ultraviolat-visible (UV-Vis) absorption spectra were obtained using a Shimadzu UV-3600 equipment. The UV-Vis presented a total wavelength range of 185-3300 nm with a resolution of 0.1 nm. The equipment was operated using an integrating sphere ISR-3100 accesory with an inner diameter of ~60 mm PMT and PbS sensors. The optical range of the accessory was 220-2600 nm.

CO_2 fixation reaction

The reactor consists in an inert reaction chamber coated with a perfluorinated polymer (120 mL) where both the catalyst and water were incorporated. The reactor was equipped with an inlet valve for the entrance of gases and an outlet valve to recover the gaseous reaction products. A UV lamp (GPH265T5L/4, 253.7 nm) was also placed in the middle of the reactor to irradiate the catalyst directly, the lamp being protected by a UV transparent quartz tube. All surfaces were coated with a thin film of a perfluorinated polymer in order to avoid any contact between the reaction medium and the reactor

surfaces, in this way discarding other catalytic effects. Reaction conditions for each studied process are described in the main text.

The reaction products were analyzed by ^{1}H NMR spectroscopy. All^{1}H NMR spectra were acquired with a Bruker Avance III-400 spectrometer operating at 400.1 MHz. The chemical shift was calibrated using tetramethylsilane as internal standard. 256 scans were recorded in all cases. In order to extract the products from the catalyst, samples were dissolved in milli-Q water containing 100 mM of HCl and 50 mM of NaCl with the final addition of deuterated water.

Distinction of the parameters used to weight the scale of reaction conditions

Catalyst natural abundancy axis has been assigned in each study by taking the catalyst less abundant element on Earth's crust54, in % w/w. For the Conditions Harshness axis, reaction temperature from 0-1000 ºC scored from 0 to 4 a.u. points; reactions involving an additional requirement (i. e. thermal pre-treatment, UV light, voltage power supply), added extra 0.5 a.u. points. Thus, studies were rated from mild to very hard conditions depending on the final score obtained. In absolute value: mild (0-1), medium (1-2), hard (2-3) and very hard (3-4).

RAMAN SPECTRA DISCUSSION & PEAK ASSIGNATION

TiO_2

The TiO_2 provides two distinguishable vibrational fingerprints depending on the its crystallographic phase. On one hand, anatase phase is characterized by four modes located at 143, 396, 516 and 640 cm^{-1} which corresponds to the Ti–O double degenerated modes, Ti–Ti single degenerated vibrations, single degenerated oxygen vibrations and Ti–O double

degenerated modes, respectively.[S1-S3] On the other hand, rutile presents two peaks at 447 and 610 cm^{-1}, which have been attributed to the oxygen-atom free vibrations in the lattice.[S1-S3] As expected, s-TiO_2 (presented in the main text, Figure 1a) has undergone to a phase transition from anatase (< 500 ºC) to rutile. Accordingly, for s200-(s-HAp/TiO_2) and s400-(s-HAp/TiO_2) samples sintered at 200 and 400 ºC, respectively (Figure S3) the anatase phase can be clearly identified. Moreover, the full width at half maximum (FWHM) of the main TiO_2 slightly increases at 400 ºC, anticipating the phase transition to rutile.

$CaTiO_3$

The Raman active modes of $CaTiO_3$ located at 182, 227, 248, 289, 339, 471 and 495 cm^{-1} have been attributed to the O–Ti–O motion of A-sites, 2nd to 5th modes are identified with O–Ti–O bending and the latter ones with Ti–O_3 torsional modes.[S5-S6]

HAp

s-HAp spectrum (Figure 1a) is characterized by four vibration modes located at v_1 = 962, v_2 = 400-480, v_3 = 570625 and v_4 = 1020-1095 cm^{-1}, corresponding to the symmetric stretching mode of the P–O bonds, the double degenerate O–P–O bending mode, the triply degenerate asymmetric P–O stretching mode, and the triply degenerate O-P-O bending mode, respectively.[S7] Accordingly, the well-resolved modes in conjunction with the fact that the main vibration peak v_1 does not present any splitting (attributed to the existence of lattice distortions or other calcium phosphate salts) confirms the presence of highly pure and crystalline HAp.

Although exhaustive characterization of p-HAp has been carried out by means of a combinations of different spectroscopic and morphological techniques,[S7-S9] Raman spectra

has been shown to provide valuable and fast information which can be used as controls. More specifically, the optimum generation of vacancies (through the sintering/dehydration process) can be checked by integrating the stretching vibration of ν-OH peak at 3574 cm^{-1} (visible using the 532 nm rather than the 785 nm laser). Thus, the hydroxyl content (A_{OH}) has been determined as the ratio of the integrated peaks at 3574 and 962 cm^{-1}. Figure S1 presents the Raman spectra focusing in the hydroxyl vibration region for s-HAp, s-(s-HAp/TiO_2) and s-HAp/TiO_2 samples. The A_{OH} values obtained (0.21 ± 0.01, 0.18 ± 0.01, and 0.11 ± 0.01, respectively) confirms that the presence of TiO_2 do not affect the proper generation of hydroxyl vacancies for all samples. As it has been aforementioned, FHWM measurement of the main peak vibration (for HAp the ν_1) is useful to detect the presence of distortions in the lattice, and thus can be used as a semi-quantitative approach to crystallinity.[S7,S8] According to the Figure 1 s-HAp and s-(s-HAp/TiO_2) present similar FWHM values ~8,1 cm^{-1}. Note that s-HAp/TiO_2 has been discarded due to the complete TiO_2 degradation and the existence of significant HAp lattice distortions. Successful p-HAp state can be detected by the superficial generation of hydroxyl-stabilized brushite phase (applies when the TSP treatment is performed using separate electrodes at 500 V and 1000 ºC),[S10] which present characteristic vibration peaks at 878, 844 and 794 cm^{-1} corresponding to the HPO_4^{2-} normal vibration mode, and the POH deformation and rotation modes characteristic of brushite.

REFERENCES

[S1] CRC Handbook of Chemistry and Physics.

[S2] U. Balachandran and N. G. Eror, *J. Solid State Chem.*, 1982, **42**, 276-282.

[S3] O. Frank, M. Zukalova, B. Laskova, J. Kürti, J. Kolati and L. Kavan, *Phys. Chem. Chem. Phys.,* 2021, **14**, 14567-14572.

[S4] V. Swamy, B. C. Muddle and Q. Dai, *Appl. Phys. Lett.*, 2006, **89**, 163118.

[S5] H. Zheng, G:D:C Csete de Györgyfalva, R. Quimby, H. Bagshaw, R. Ubic, I. M. Reaney and J. Yarwood, *J. Eur. Ceram. Soc.*, 2003, **23**, 2653-2659.

[S6] U. Balachandran and N. G. Eror, *Solid State Commun.*, 1982, **44** 815-818.

[S7] J. Sans, J. Llorca, V. Sanz, J. Puiggalí, P. Turon and C. Alemán, *Langmuir*, 2019, **35**, 14782-14790.

[S8] J. Sans, M. Arnau, F. Estrany, P. Turon and C. Alemán, Regulating the superficial vacancies and OH- orientations on polarized hydroxyapatite electrocatalysts, Adv. Mater. Interfaces, 8 (2021) 1-10.

[S9] J. Sans, M. Arnau, V. Sanz, P. Turon and C. Alemán, Fine.tuning of polarized hydroxyapatite for the catalytic covnersion of dinitrogen to ammonium under mild conditions, Chem. Eng. J. 433 (2022) 133512.

[S10] J. Sans, M. Arnau, V. Sanz, P. Turon and C. Alemán, Polarized hydroxyapatite : New insights and future perspectives through systematic electrical characterization at the interface, Adv. Mater. Interfaces, 9 (2022) 2101631.

s-(X)	Accounts for a material or mixture from where a sintering treatment has been applied (1000 ºC for 2 hours).
p-(X)	Accounts for a material or mixture from where the TSP treatment has been applied (500 V, 1000 ºC for 1 hour).
HAp/TiO_2	Powder mixture of HAp/TiO_2 (the percentage of TiO_2 is specified in the text). The mixtures are latterly compressed into discs.
p-HAp	Compressed HAp disc composed of sintered HAp (s-HAp) which has been latterly polarized through the TSP treatment.
C-HAp/TiO_2	Optimized catalyst prepared as sketched in Scheme 1: compressed s-HAp from where drop casting of TiO_2 NPs has been applied (6.6 mg/L). Finally, the TSP treatment has been applied.
S500-(HAp/TiO_2)	Compressed HAp disc from where drop casting of TiO_2 NPs has been applied (6.6 mg/L). Sintering treatment submitting the sample at 500 ºC for 2 hours has been applied

Table S1. Experimental methods and references for the samples prepared in this work.

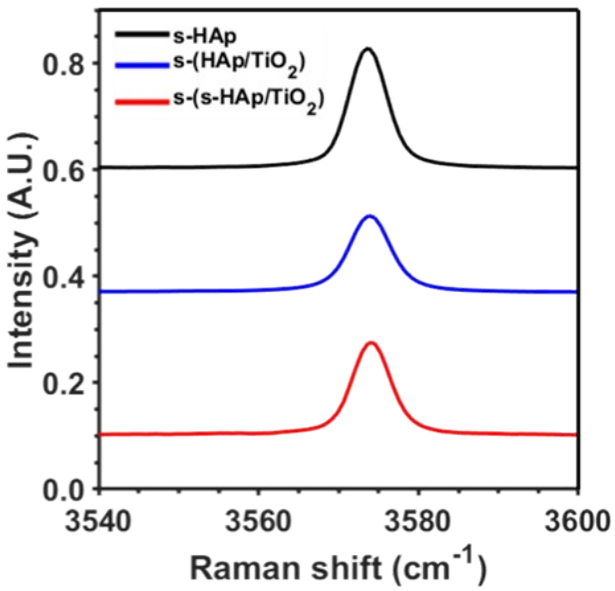

Figure S1. Raman spectra of s-HAp, s-(HAp/TiO_2) and s-(sHAp/TiO_2) samples in the ν-OH region. Changes in the area (normalized) in the three peaks can be extrapolated to the dehydration of OH^- groups.

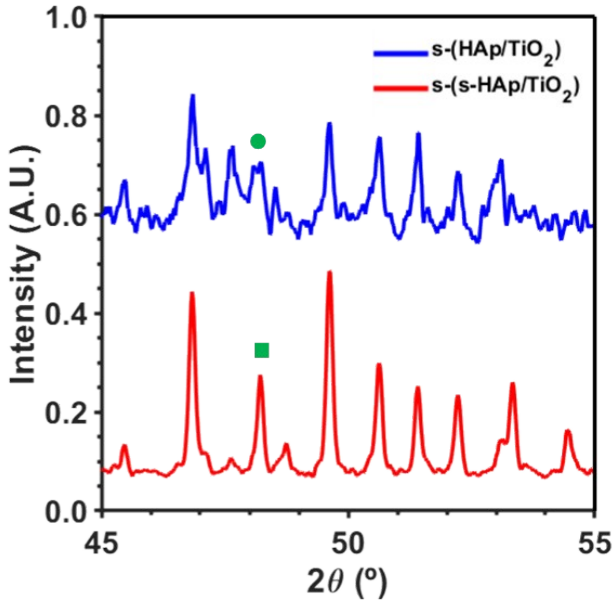

Figure S2. Figure 1b inset. WAXD spectra of the samples containing $CaTiO_3$ and TiO_2. As it can be observed with the circle and square marls, if not paying careful attention, the overlap of two peaks could lead to an incorrect interpretation of the crystallographic planes.

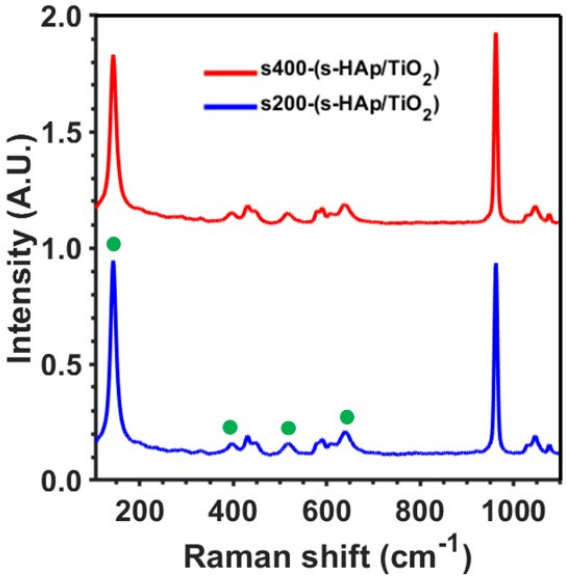

Figure S3. Raman spectra of the two samples sintered below TiO_2 phase transition temperature. The circular points indicate the main peaks of TiO_2 anatase phase.

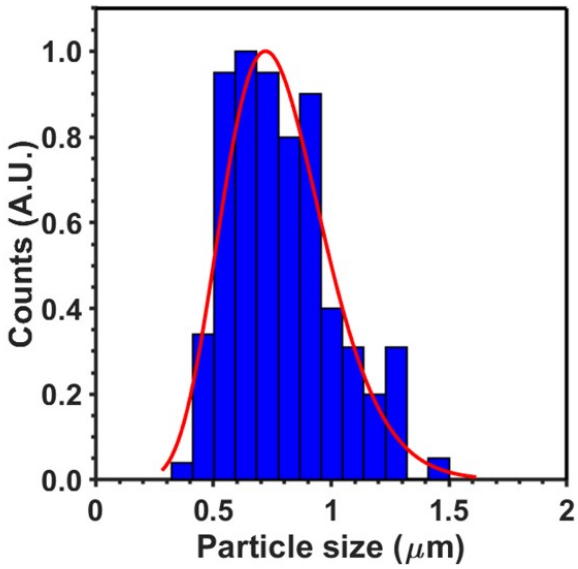

Figure S4. DLS measurement of TiO_2 size distribution when performed a suspension in PBS and at pH = 7.

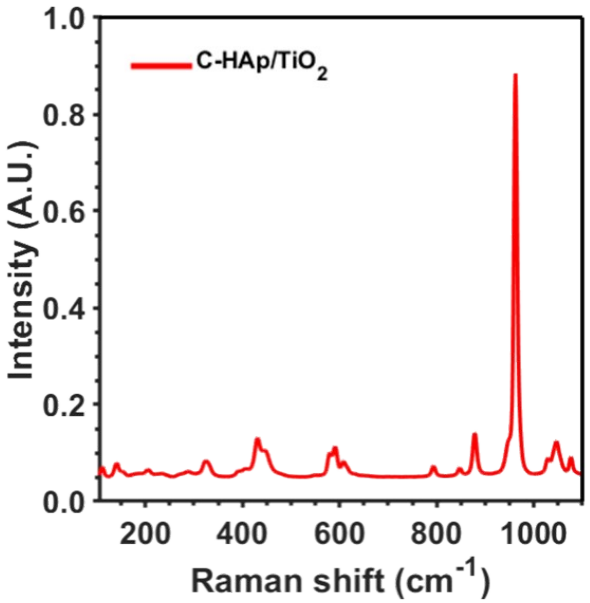

Figure S5. Raman spectra of C-HAp/TiO_2 where the previous identified rutile peaks cannot be observed due to its low content.

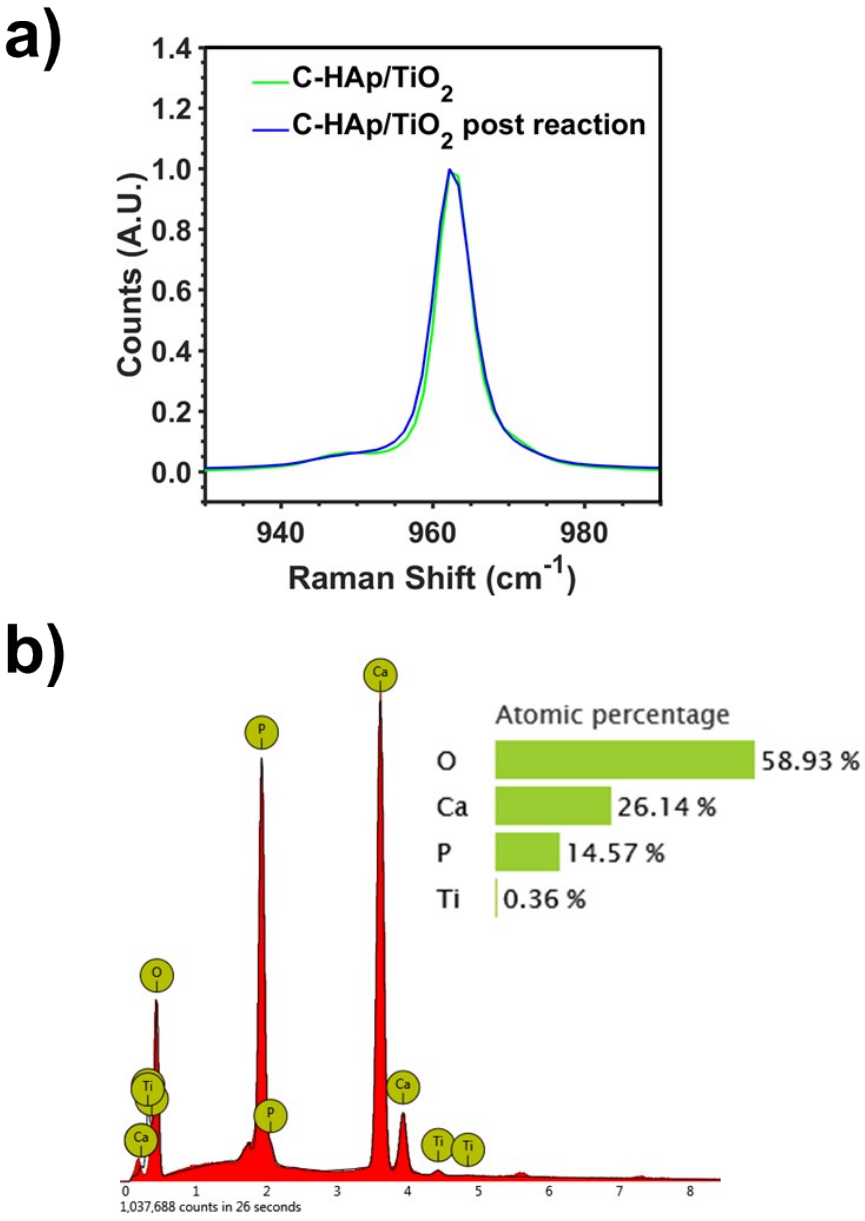

Figure S6. Structural stability of the C-HAp/TiO_2 after the reaction. (a) Raman peak of the main vibration mode v_1 of p-HAp. As it can be observed no distortion on the p-HAp crystal lattice has been detected. (b) Energy-Dispersive X-ray (EDX) measurement demonstrating the presence and proper adhesion of TiO_2 NPs on the surface of the catalyst after the reaction

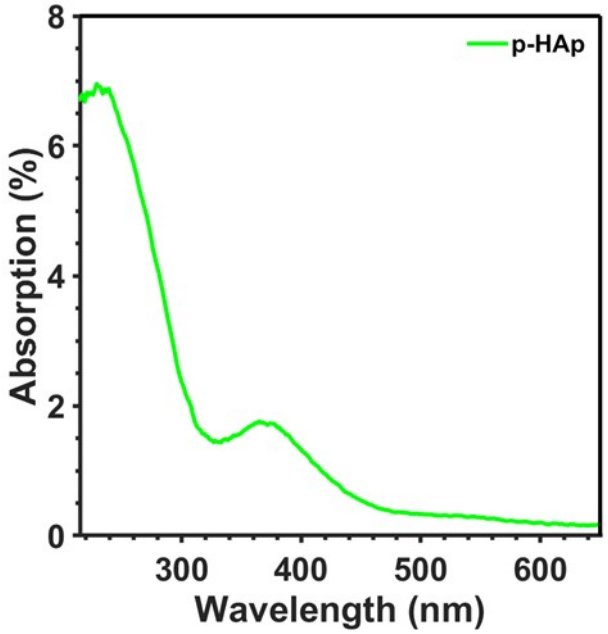

Figure S7. UV-Vis absorption spectrum of p-HAp.

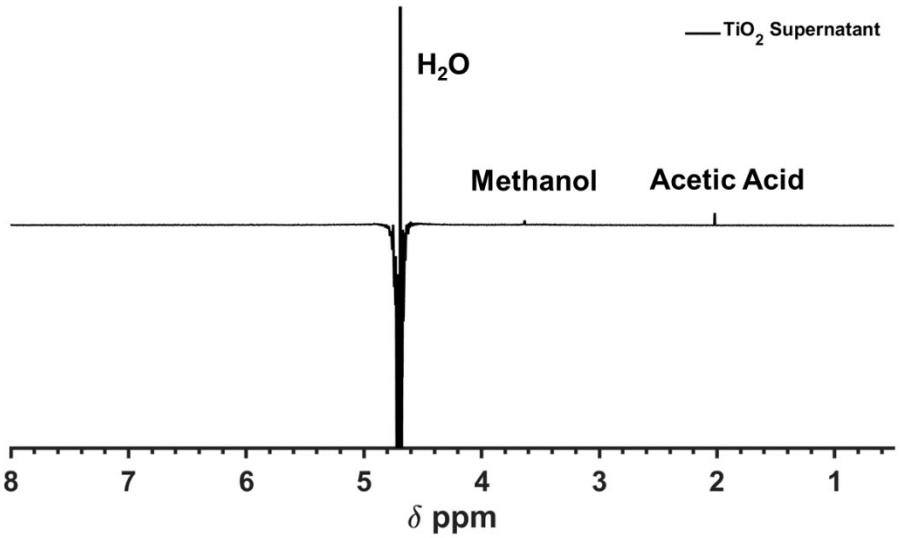

Figure S8. ^{1}H NMR spectrum of the reaction carried out using TiO_2 as catalyst and under the same reaction conditions reported in this work.

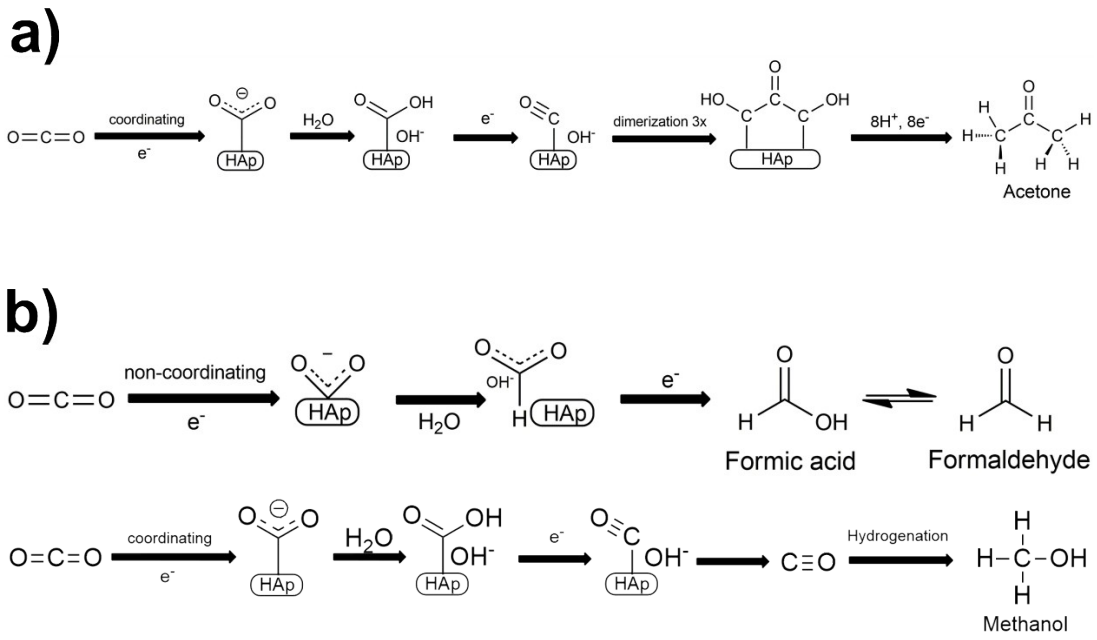

Scheme S1. Proposed mechanisms for other C3 (acetone S1a) and C1 (formaldehyde and methanol S1b) products.